Epidemics 47 (2024) 100757

Contents lists available at ScienceDirect

Epidemics

journal homepage: www.elsevier.com/locate/epidemics

A multiscale modeling framework for Scenario Modeling: Characterizing the heterogeneity of the COVID-19 epidemic in the US

Matteo Chinazzi [a,b,1], Jessica T. Davis [b,1], Ana Pastore y Piontti [b], Kunpeng Mu [b], Nicolò Gozzi [c], Marco Ajelli [d], Nicola Perra [e,b], Alessandro Vespignani [b,c,*]

[a] The Roux Institute, Northeastern University, Portland, ME, USA
[b] Laboratory for the Modeling of Biological and Socio-technical Systems, Network Science Institute, Northeastern University, Boston, MA, USA
[c] Institute for Scientific Interchange Foundation, Turin, Italy
[d] Laboratory for Computational Epidemiology and Public Health, Department of Epidemiology and Biostatistics, Indiana University School of Public Health, Bloomington, IN, USA
[e] School of Mathematical Sciences, Queen Mary University, London, UK

ARTICLE INFO

Dataset link: https://coronavirus.jhu.edu/, https://www.oag.com/, https://www.iata.org/, https://www.google.com/covid19/mobility/, https://github.com/OxCGRT/covid-policy-tracker

Keywords:
Metapopulation dynamics
Multi-strain epidemic modeling
COVID-19 pandemic

ABSTRACT

The Scenario Modeling Hub (SMH) initiative provides projections of potential epidemic scenarios in the United States (US) by using a multi-model approach. Our contribution to the SMH is generated by a multiscale model that combines the global epidemic metapopulation modeling approach (GLEAM) with a local epidemic and mobility model of the US (LEAM-US), first introduced here. The LEAM-US model consists of 3142 subpopulations each representing a single county across the 50 US states and the District of Columbia, enabling us to project state and national trajectories of COVID-19 cases, hospitalizations, and deaths under different epidemic scenarios. The model is age-structured, and multi-strain. It integrates data on vaccine administration, human mobility, and non-pharmaceutical interventions. The model contributed to all 17 rounds of the SMH, and allows for the mechanistic characterization of the spatio-temporal heterogeneities observed during the COVID-19 pandemic. Here we describe the mathematical and computational structure of our model, and present the results concerning the emergence of the SARS-CoV-2 Alpha variant (lineage designation B.1.1.7) as a case study. Our findings show considerable spatial and temporal heterogeneity in the introduction and diffusion of the Alpha variant, both at the level of individual states and combined statistical areas, as it competes against the ancestral lineage. We discuss the key factors driving the time required for the Alpha variant to rise to dominance within a population, and quantify the impact that the emergence of the Alpha variant had on the effective reproduction number at the state level. Overall, we show that our multiscale modeling approach is able to capture the complexity and heterogeneity of the COVID-19 pandemic response in the US.

1. Introduction

Mathematical and computational models have been essential in understanding the transmission mechanisms of SARS-CoV-2, providing situational awareness throughout the COVID-19 pandemic, and allowing the exploration of hypothetical intervention scenarios for public health planning and response (Holmdahl and Buckee, 2020; Jewell et al., 2020; Poletto et al., 2020; Brooks-Pollock et al., 2021; Biggerstaff et al., 2022; Reich et al., 2022). Despite the many successful applications of predictive modeling, there are often challenges in communicating the results to policymakers and the public due to poor coordination among modeling teams, divergent results caused by different underlying assumptions and scenarios, and a lack of clarity regarding the implemented methods. To address these issues, the Scenario Modeling Hub (Scenario Modeling Hub, 2023) has coordinated multiple modeling teams in the generation and analysis of multi-model projections of well-defined epidemic scenarios (Borchering et al., 2021; Biggerstaff et al., 2022; Truelove et al., 2022; Howerton et al., 2023; Borchering et al., 2023). This hub approach allows for a synoptic analysis of results, ensembling different estimates, rigorous validation of findings, and clearer communication of results.

* Corresponding author at: Laboratory for the Modeling of Biological and Socio-technical Systems, Network Science Institute, Northeastern University, Boston, MA, USA.
E-mail address: a.vespignani@northeastern.edu (A. Vespignani).
[1] Authors contributed equally.

https://doi.org/10.1016/j.epidem.2024.100757
Received 15 August 2023; Received in revised form 22 January 2024; Accepted 26 February 2024
Available online 5 March 2024

As of July 2023, we have contributed 17 rounds of projections coordinated by the SMH, which consist of 70 different modeling scenarios defined at various points in time starting in 2021. Our modeling approach combines two stochastic, age-structured, multi-strain, metapopulation models operating on different scales (Balcan et al., 2010). This approach allows us to model both the local dynamics that integrate the vaccination rollout plans and the strength of non-pharmaceutical interventions (NPIs) as well as the global dynamics responsible for the introduction of new variants. In particular, the Global Epidemic and Mobility model (GLEAM) which has been used to study the international spread of pathogens such as Zika (Zhang et al., 2017), Ebola (Gomes et al., 2014; Pastore y Piontti et al., 2016), and the initial wave of COVID-19 (Chinazzi et al., 2020; Davis et al., 2021), can simulate introduction events of new variants in the United States (US) from other countries. The output of this model is used to define the initial conditions of the Local Epidemic and Mobility model (LEAM-US) that in turn simulates the disease dynamics in the US at the county level.

Here we describe our general modeling approach and report the detailed results obtained following the guidelines of the scenario design of Round 5 of the SMH (COVID-19 Scenario Modeling Hub, 2021). The four scenarios of this round address the impact of vaccination coverage and relaxation of NPIs during the wave initiated by the Alpha variant (Phylogenetic Assignment of Named Global Outbreak, PANGO, lineage designation B.1.1.7). The Alpha variant was first identified in December 2020 in the United Kingdom (UK) (Walensky et al., 2021; World Health Organization, 2021). It was traced back to two samples collected in September 2020 (Science Magazine, 2020; Rambaut et al., 2020). The multiscale structure of our model and its capacity to link international importations with domestic contact patterns and mobility, provides a detailed characterization of the heterogeneous spread of the Alpha variant in the US. We estimate that its introduction and trajectory towards dominance exhibited significant spatiotemporal variation. In particular, our model finds that by March 2021 the Alpha variant accounted for 50% or more of the total infections only in roughly one third of states. In contrast, other states did not reach this proportion until the end of April or early May. Notably, this heterogeneity is even more pronounced at the combined statistical areas (CSAs) level within states. Additionally, we show how the emergence of the Alpha variant affected variations in the effective reproduction number at the state level.

Overall, our multiscale model offers a comprehensive and detailed approach to projecting the COVID-19 pandemic in the US, incorporating factors such as population demographics, travel patterns, NPIs, vaccination status, and new SARS-CoV-2 variants. These projections can inform public health policy and decision-making by capturing the heterogeneity and complexity of the COVID-19 pandemic response in the US.

2. Methods

The multiscale modeling approach combines two distinct epidemic models that work at different geographical resolutions: the Global Epidemic and Mobility model (GLEAM) and the Local Epidemic and Mobility model in the US (LEAM-US) (Fig. 1). Both models are stochastic, spatial, age-structured, metapopulation models (Balcan et al., 2009, 2010; Pastore y Piontti et al., 2018; Chinazzi et al., 2020). LEAM-US, considers 3142 counties (or their statistical equivalent) as individual subpopulations in each of the 50 US states and the District of Columbia. GLEAM considers 3200 subpopulations across nearly 190 countries, defined as catchment areas of major transportation hubs. GLEAM and LEAM-US integrate a human mobility layer, represented as a network, using both short-range (i.e., commuting) and long-range (i.e., air traveling) mobility data from different sources. International and domestic airline mobility data, in the origin–destination format, are from the Official Aviation Guide database and are used to model airline transportation (OAG, 2020). Ground mobility and commuting flows are modeled from data collected from statistics offices of 30 countries on 5 continents and account for travel restrictions and government policies (Hale et al., 2021). The model also considers the reduction of internal country-wide mobility and changes in contact patterns in each country and state (Google LLC, 2021a). In both models we consider individuals divided into 10 age groups: 0–9, 10–19, 20–24, 25–29, 30–39, 40–49, 50–59, 60–69, 70–79, and 80+ years old. We use effective contact matrices to model age-dependent and country/state specific mixing across four settings: households, schools, workplaces, and contacts occurring in the general community. The contact matrix for a given location is a weighted linear combination of the derived matrices for the four social settings and encodes information on the average number of *effective* contacts (contacts that can lead to the transmission of a disease) between individuals of particular age groups. Details on the contact data and the construction of the matrices can be found in Mistry et al. (2021) and Prem et al. (2017).

In the LEAM-US model, contact matrices, age-specific traveling probabilities, and air traffic flows are properly mapped to the county-level resolution. Counties' populations and age distributions are based on the Census' annual resident population estimates during 2019, and commuting flows between counties are obtained from the 2011–2015 5-Year ACS Commuting Flows survey and properly adjusted to account for differences in population totals since the creation of the dataset (US Census Bureau, 2024). Google's COVID-19 Community Mobility Reports data collected at the county-level resolution are used to model mobility and the effects of NPIs on individual behaviors (Google LLC, 2021a).

2.1. SARS-CoV-2 transmission model

In both GLEAM and LEAM-US, within each subpopulation, we adopt a classic $SLIR$-like disease infection dynamics. Depending on the SMH round, the model has been extended to account for the presence of multiple lineages and vaccination protocols. After establishing the mobility data layers and defining the dynamics of the disease, the population count within each compartment, denoted as m, for each age group i, and for each subpopulation j, is governed by a discrete and stochastic dynamical equation. This equation is formulated as follows:

$$X_j^{[m,i]}(t+\Delta t) - X_j^{[m,i]}(t) = \Delta X_j^{[m,i]} + \Omega_j([m,i]) \tag{1}$$

where the term $\Delta X_j^{[m,i]}$ denotes the change attributable to transitions within compartments, which are driven by the dynamics of disease transmission. Additionally, the operator $\Omega_j([m,i])$ captures the variations arising from individual mobility. This particular operator accounts for long-range mobility, specifically via airlines, and establishes the minimal integration time scale as one day. Finally, the impact of commuting flows on mobility is incorporated by defining effective forces of infection. This is achieved through a time scale separation approximation detailed in Balcan et al. (2010), Balcan and Vespignani (2011). The function $\Delta X_j^{[m,i]}$ is defined as the aggregate of all transitions into and out of the disease compartment m for individuals within age group i, denoted as $[m,i]$. The operator $Dj([m,i],[n,i])$ quantifies the transitions from $[m,i]$ to $[n,i]$ over the time interval Δt. Each element of this operator is derived as a random variable, following a multinomial distribution. Therefore, the change in the compartment $[m,i]$ over the interval Δt, represented as $\Delta X j^{[m,i]}$, is calculated by summing all the random variables $\{D_j([m,i],[n,i])\}$ as follows

$$\Delta X_j^{[m,i]} = \sum_{[n,i]} \left\{ -D_j([m,i],[n,i]) + D_j([n,i],[m,i]) \right\}. \tag{2}$$

To illustrate the above equation with a specific example, let us inspect the dynamics of the latent compartment. Consider individuals within age group i of subpopulation j. These individuals have two potential transitions: they can either move into the latent compartment, denoted as L_j^i, from the susceptible compartment, represented

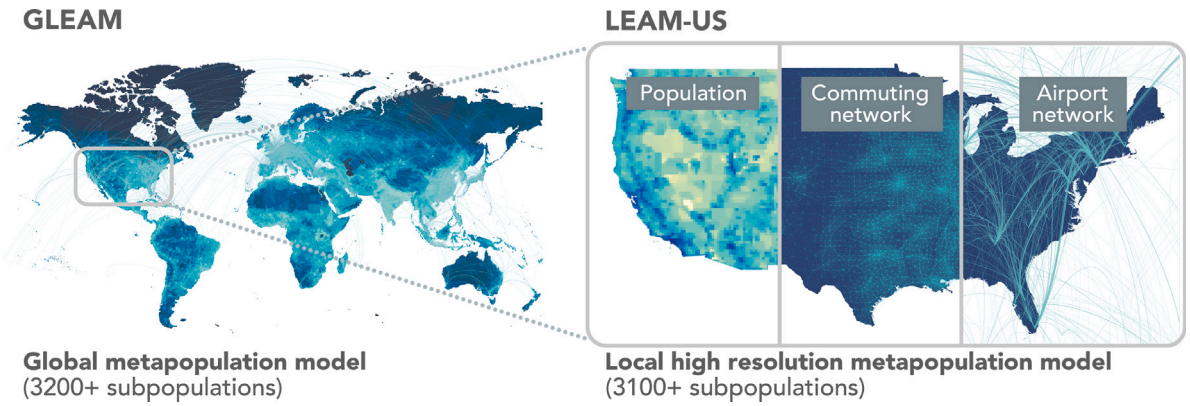

Fig. 1. Visual depiction of the multiscale modeling approach that combines the GLEAM and LEAM-US models.

as S_j^i, or they can exit the latent compartment to enter the infectious compartment, indicated by I_j^i. The components of the operator that define the L_j^i dynamic are thus determined by the following binomial distributions $Pr^{Bin}(L_j^i(t), p_{L_j^i \to I_j^i})$ and $Pr^{Bin}(S_j^i(t), p_{S_j^i \to L_j^i})$, where $p_{L_j^i \to I_j^i}$ and $p_{S_j^i \to L_j^i}$ are the transition probabilities from the latent to the infectious state and from the susceptible to the latent state, respectively. We model the transition process as memoryless, discrete, and stochastic. The transition probability $p_{S_j^i \to L_j^i}$, representing the force of infection, is influenced by several factors: commuting flows, interaction patterns as defined in age-structured contact matrices, and the implementation of local Non-Pharmaceutical Interventions (NPIs). For a complete description of the analytical framework of the model, we direct readers to the detailed presentation provided in Balcan et al. (2010).

In the removed compartment, individuals can no longer infect others, meaning they have either recovered, been hospitalized, or isolated. Hospitalizations and deaths are computed from the removed compartment by considering a geometrically distributed time delay between the time of removal to hospitalization and death (details on the delay implementation are provided in the Supplementary Information). Infection hospitalization ratios (IHR) and infection fatality ratios (IFR) are age-structured and taken from the literature to account for different variants and vaccination statuses (Shapiro et al., 2021; Verity et al., 2020; Salje et al., 2020). It is worth remarking that the model's parameters vary across SMH rounds as new variants and knowledge on vaccine efficacy emerged and as the prescribed scenarios changed.

2.2. Non-pharmaceutical interventions and human mobility

In our model, we dynamically incorporate international travel restrictions based on data from the Oxford COVID-19 Government Response Tracker (Hale et al., 2021). To accurately reflect changes in travel patterns since the pandemic's onset, both international and domestic travel flows are adjusted using real-time origin–destination data provided by OAG (OAG, 2020), capturing the observed reductions in air traffic. Additionally, we adjust short-range mobility by utilizing workplace visitation data as a proxy. This approach, that consider the mobility changes from pre-pandemic levels, is informed by Google's COVID-19 Community Mobility Reports (Google LLC, 2021a), and provides a dynamic characterization of mobility patterns during the pandemic. Contact patterns and mixing rates among different age groups in our model are adjusted to reflect the impact of policy interventions on individual behaviors. Specifically, we modulate the school contacts matrix layer to simulate the effects of school closures, whether due to governmental policies or scheduled holiday breaks. For workplace and general community settings, we utilize data from Google's Mobility Reports. The `workplaces percent change from baseline` metric informs us of the reduction in contacts within workplaces, while the `retail and recreation percent change from baseline` gives insights into contact reductions in broader community settings. We achieve this by proportionally rescaling the corresponding layers in the contact matrices. This rescaling factor, $\omega_s(t) = \omega_s(1 + r_l(t)/100)^2$, is applied, where $r_l(t)$ represents the daily percentage change in visitors to specific locations s relative to pre-pandemic levels. The squared term in this factor reflects the understanding that the potential number of contacts at a location is proportional to the square of the visitor count. We selected specific fields from Google's Community Mobility Report data due to their alignment with the definitions of various place categories. The 'retail and recreation percent change from baseline' field effectively represents mobility trends for locations such as movie theaters, restaurants, cafes, and shopping centers. This particular data is most representative of the interactions occurring within the general community layer of our contact matrices. Meanwhile, the 'workplaces percent change from baseline' field is instrumental in measuring the mobility trends of individuals commuting to and from their workplaces, providing valuable insights for our modeling purposes (Google LLC, 2021b).

2.3. Vaccine allocation and administration

Our model explicitly incorporates the time series data of daily administered COVID-19 vaccine doses. In the United States, the allocation of the daily vaccine stockpile for each county is based on the observed vaccination rates at the state level. We then distribute these doses within each state, proportionally to the population size of each county. Furthermore, the strategy for vaccine rollout is designed to align with the recommendations of the Advisory Committee on Immunization Practices (ACIP). This approach involves prioritizing different age groups in a phased manner, depending on the specific stage of the vaccination campaign (Dooling et al., 2020). In particular, in phase 1a doses were distributed between the 10 age groups according to the number of healthcare workers and long-term care facility residents in the population; in phase 1b they were distributed with priority to front-line essential workers and adults aged 75+; in phase 1c to other essential workers, adults with high-risk conditions, and the 65–74 age group; and lastly, in phase 2, doses were distributed to the general population aged 18+. The vaccine uptake in the in-sample calibration window follows the data provided by the CDC and Our World in Data platform (CDC, 2021; Our World in Data, 2021). In the out-of-sample projection period, the vaccine uptake of each SMH round follows the directions of the specific scenarios, available at COVID-19 Scenario Modeling Hub (2021). Our model incorporates various vaccine effects, including vaccine efficacy in reducing the risk of infection (VE^S), hospitalization (VE^H), and deaths (VE^D). The specific values for these vaccine efficacies vary across different scenario rounds and are informed by the ongoing analysis of efficacy against different variants. Additionally, the model accounts for the waning of vaccine-induced protection starting from round 8.

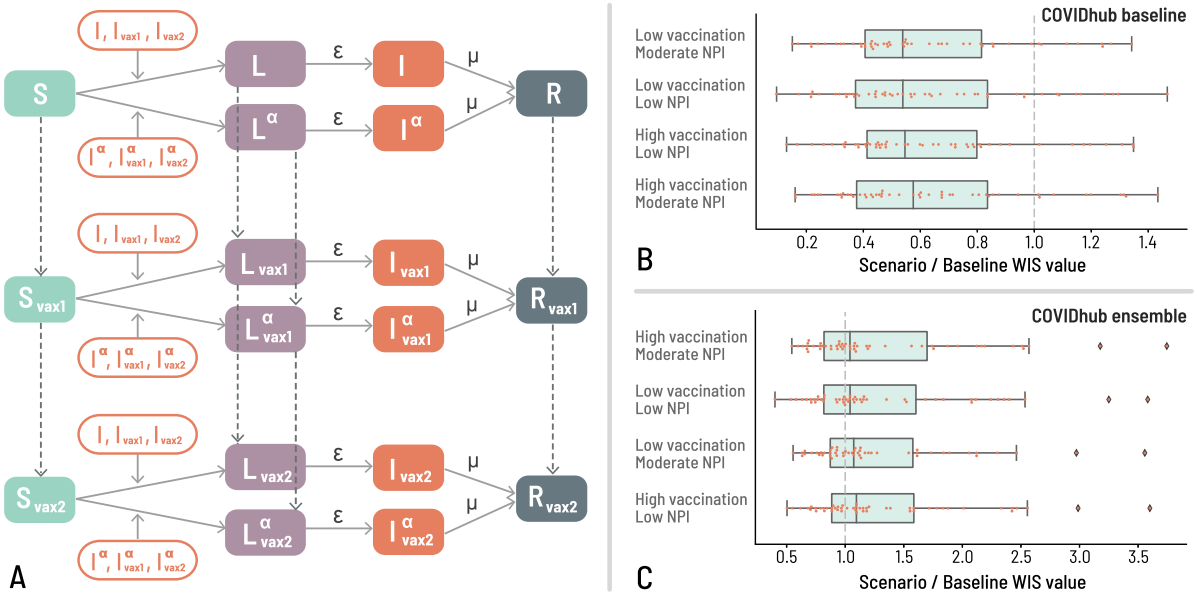

Fig. 2. (A) We implement a $SLIR$-like model extended to account for the presence of two strains and vaccination. The superscript α refers to compartments with individuals infected with the Alpha variant of concern. Subscripts $vax1$ and $vax2$ are used to identify compartments with individuals who received one or two doses of the vaccine, respectively. Vertical dashed lines represent transitions between compartments due to vaccinations. (B) Ratios of WIS scores between the GLEAM/LEAM-US model and the COVIDhub baseline reference model. (C) Ratios of WIS scores between the GLEAM/LEAM-US model and the COVIDhub ensemble reference model.

2.4. Model calibration

The model is initialized by considering the introductions of infections during the early stage of the COVID-19 pandemic by coupling the LEAM-US model to the importations from the GLEAM model calibrated as reported in Davis et al. (2021). In each state, we assume a flat prior for the effective reproductive number R_{eff} at the start of the in-sample calibration time window. In order to account for variations in the IFR and IHR across states, we also consider a $\pm$ 30% difference with respect to the baseline parameterization, assuming a uniform prior. The specifications set by the SMH in each round inform the time window used to calibrate the model. We calibrate our model using an Approximate Bayesian Computation (ABC) rejection approach (Sunnåker et al., 2013). This process involves comparing the model's weekly estimated deaths and/or hospitalizations with the actual figures reported by the Johns Hopkins Coronavirus Resource Center (Dong et al., 2020) and the U.S. Department of Health and Human Services (US Department of Health & Human Services, 2021). To assess the accuracy of our model, we calculate the distance, denoted as $s(E', E)$, between the surveillance data (evidence E) and the model estimates (E') for each stochastic realization. Distances are measured using either the weighted mean absolute percentage error or the residuals. We then establish a tolerance level, based on a selected quantile of the empirical distance distribution, to serve as our threshold. Any realizations that result in distances exceeding this threshold are rejected (Beaumont et al., 2002). Specifically, we keep the top 2.00% of realizations with the smallest distance. For each specific SMH-scenario definition, we performed between 15,000 to 50,000 stochastic independent realizations. We have also performed extensive sensitivity analyses testing the calibration approaches at the global and local level as reported in Davis et al. (2021).

2.5. Round 5 specific model design: Integrating the alpha variant

To incorporate the emergence of the Alpha variant mechanistically we employ a two-strain model. This model allows us to mechanistically capture the cocirculation of the ancestral SARS-CoV-2 lineages and the Alpha variant. The model considers the following compartments: susceptible; two latent and infectious compartments (capturing individuals infected with both the ancestral lineages and the Alpha variant); and the removed compartments. Additionally, each of the previous compartments appears in the model in three different ways (as shown in Fig. 2A) to distinguish between unvaccinated individuals, individuals who received the first vaccine dose, and vaccinated individuals who received two doses. Susceptible (S) individuals become latent through interactions with infectious individuals carrying either the ancestral lineage or the variant. In the first case, individuals will transition into the ancestral lineage latent compartment (L); in the second they will transition into the variant latent compartment (L^α). We assume that the two lineages have different transmission rates (β and β^α) but the same latent and infectious periods (ε^{-1} and μ^{-1}). Furthermore, we capture the increase in transmissibility of the Alpha variant by assuming that $\beta^\alpha = \beta(1+\psi)$ (Galloway et al., 2021). The increase of transmissibility was introduced following previous studies indicating that the Alpha variant was 30%–70% more transmissible with respect to ancestral SARS-CoV-2 lineages (NERVTAG, 2020; PHE, 2021; Davies et al., 2021). Latent individuals move to the infectious stage, I for the ancestral lineage and I^α for the Alpha variant, at a rate ε that is inversely proportional to the latent period. Infectious individuals transition to the removed compartment (R) at a rate μ that is inversely proportional to the infectious period. In our model, individuals transition between different compartments through stochastic binomial chain processes. These transitions are guided by parameter values sourced from existing literature, which outline the natural progression of the disease. During the period of our projections, the vaccination campaign was focused on administering the initial complete regimen of two doses. Accordingly, our model accounts for varying levels of vaccine efficacy against infection, hospitalization, and death, distinguishing between the effects after the administration of the first and second doses. In collaboration with the SMH, the vaccine efficacy (VE) values for one dose and two doses were established at 70% and 90% for susceptibility to infection (VE^S), and 75% and 95% for both hospitalization (VE^H) and deaths (VE^D). It is important to note that during the scenario design phase, detailed information on vaccine efficacy was limited, except for the efficacy against symptomatic disease, which was informed by phase 3 trials (Polack et al., 2020; Pilishvili et al., 2021). The protection conferred by the vaccination for the Alpha variant was assumed to be

similar to those of the ancestral lineages, after considering the increased transmissibility.

The assumptions of the future levels of NPIs and vaccination uptake were incorporated based on the scenarios presented by the SMH. A full description of all scenarios can be found at this link (COVID-19 Scenario Modeling Hub, 2021). In round 5 we explore two scenarios that assume different levels, moderate and low, of NPIs. More precisely, starting on May 1, 2021, we consider a reduction in the effect of NPIs on mobility and contacts relative to the effectiveness of control during the last two weeks in April, 2021. The two scenarios assume a gradual reduction of social distancing measures by October 31, 2021 with respect to the April 2021 levels: an effective 50% reduction in the moderate NPI scenario, and an effective 80% reduction in the low NPI scenario. For example, if NPIs caused mobility to decrease to 50% of its pre-pandemic value at the end of April, an 80% reduction in the effectiveness of the interventions would imply a final mobility value by end of October, 2021, that would be equal to 90% of its pre-pandemic value (i.e., $0.9 = 1 - (1 - 0.5) \times (1 - 0.8)$).

Similarly, in the out-of-sample region, we consider two different scenarios for vaccine uptake. The high vaccination scenario assumes that vaccination coverage saturates at 83% of the eligible population, while the low vaccination scenario assumes a 68% coverage. These different scenarios were used to address the impact of vaccine hesitancy. Vaccination data was taken from Ref. Our World in Data (2021), CDC (2021) until May 1, 2021. Afterward, according to the SMH scenario specifications, 50 million *first* doses were available per month, following the 2-dose protocol (100 million total doses per month).

In round 5 the introduction of the Alpha variant in the US is mechanistically modeled by simulating the international spread using the GLEAM model. The GLEAM model is initialized with the introduction of a cluster of Alpha variant infections during the week of September 13–19, 2020, specifically in London and Kent, UK. These initial infections are modeled as being drawn from a Poisson distribution with a mean of 40. This approach is based on the fact that the UK was sequencing approximately 5% of positive COVID-19 cases at that time (WHO, 2020). We have incorporated into our model the assumption that the Alpha variant is 50% more transmissible than the ancestral strain, denoted by $\psi = 0.5$. From this setup, the model generates around 300,000 stochastic realizations, each tracing the movement of individuals exposed to the Alpha variant traveling to the United States. By aggregating this data, we are able to statistically characterize the timeline of the stochastic introductions of the Alpha variant into the US. This timeline is particularly important as it provides a day-by-day count of individuals traveling from various international locations to US entry points that is used at run time by the LEAM-US model as it simulates the dynamic of the Alpha wave.

3. Results

Our multiscale model has been used to generate scenario projections for all rounds of the Scenario Modeling Hub (SMH). Each round required modifications to the model to accommodate specific analyses and variations in the epidemic landscape, such as the emergence of new variants and changes in mitigation and vaccination policies. This required adapting the model during the different scenario rounds to incorporate the mechanistic description of multiple co-circulating variants (up to 4 strains), waning vaccine efficacy (after round 7), and variations in key disease progression times. The Supplementary Information (SI) provides a narrative description of the model's changes over the 10 rounds, along with a summary table of key parameters used, and an assessment of model performance. In the following, we focus on the results concerning the emergence of the Alpha variant in early 2021 (round 5 projections). We will discuss the scenario assumptions and show how our multiscale modeling approach enables us to analyze the introduction and spread of the alpha variant across the US, emphasizing the role of geographical heterogeneity.

3.1. Out of sample projections

Our model is calibrated using the complete epidemic history within the US, spanning from March 2020 to May 2021, with the calibration process based on weekly reported deaths (in-sample model estimates and goodness of fit details are provided in the SI). The model is calibrated separately for each of the four round 5 scenarios (COVID-19 Scenario Modeling Hub, 2021). We generate out-of-sample projections for the expected number of deaths and hospitalizations, along with associated uncertainties expressed as quantile ranges. These quantile ranges are determined by considering the out-of-sample dynamics of individual stochastic trajectories, selected using an ABC rejection algorithm during the in-sample calibration period. Specifically, for each scenario, our models provide target projections consisting of 23 quantiles (ranging from 0.01 to 0.99 with increments of 0.025), covering each week of the projection period. These quantiles represent expected incident hospitalizations and deaths. To facilitate the visual representation and assessment of the probabilistic estimates, the quantile projections are transformed into central prediction intervals (PIs). These prediction intervals encapsulate the model's level of confidence that future observations will fall within a specified range of values.

Evaluating scenario projections requires a fundamentally different approach compared to forecast models. While accuracy in predicting actual outcomes is the main goal in forecasts, scenario projections have different purposes. They are developed to map the range of possible epidemic dynamics, rather than to offer precise predictions. Therefore, assessing the quality of scenario projections it is not just about how closely they match the ground truth, but also about the robustness of the underlying assumptions of each scenario and the effectiveness in enveloping the spectrum of potential trajectories. The consideration of both accuracy and the quality of scenario-based assumptions is the key for scenario modeling performance evaluation. Despite these caveats, to assess the performance of scenario projections, we utilize the weighted interval score (WIS) as a performance indicator (Gneiting and Raftery, 2007; Bracher et al., 2021). The WIS considers the size and positioning of prediction intervals relative to actual outcomes. Lower WIS values indicate better forecasting performance (see SI for a discussion of WIS methodology). For comparison, we consider two reference models generated by the COVID-19 Forecast Hub: the naive baseline forecast, which predicts weekly values similar to the median of the previous week with observed fluctuations, and the ensemble forecast, aggregating predictions from all modeling teams from the Forecasting Hub (Cramer et al., 2022). Both reference models focus on four-weeks ahead predictions. We calculate the WIS for our weekly model projected incident deaths during the first six weeks of the projection period (from May 8 to June 19, 2021) for each state in the US and the District of Columbia. We compare these WIS scores with the WIS scores of the baseline and ensemble forecasting models from the COVID-19 Forecast Hub. Weeks beyond this period are excluded due to the emergence of the Delta variant, which was not considered in the scenario design. To compare the performance of the scenarios with the reference models, we compute a WIS ratio. This ratio is obtained by dividing the WIS of a given scenario and location by the WIS of the corresponding reference model. A ratio smaller than one implies a better performance of the projections with respect to the reference scenario (lower WIS). An inferior performance is indicated by a WIS ratio larger than one. The distribution of the WIS ratios of the scenario projections is presented in Fig. 2B and C for each analyzed region and scenario, comparing them against the COVIDhub baseline and 4-weeks ahead ensemble models. The WIS ratios indicate that the scenario projections outperforms the naive baseline in all scenarios and performs comparably to the four-week ahead ensemble model. The median ratios are well below one for the baseline model and close to one for the 4-week ahead ensemble, suggesting similar performance for nearly half the states performing better and the other half performing worse. No significant differences in performance are observed across scenarios,

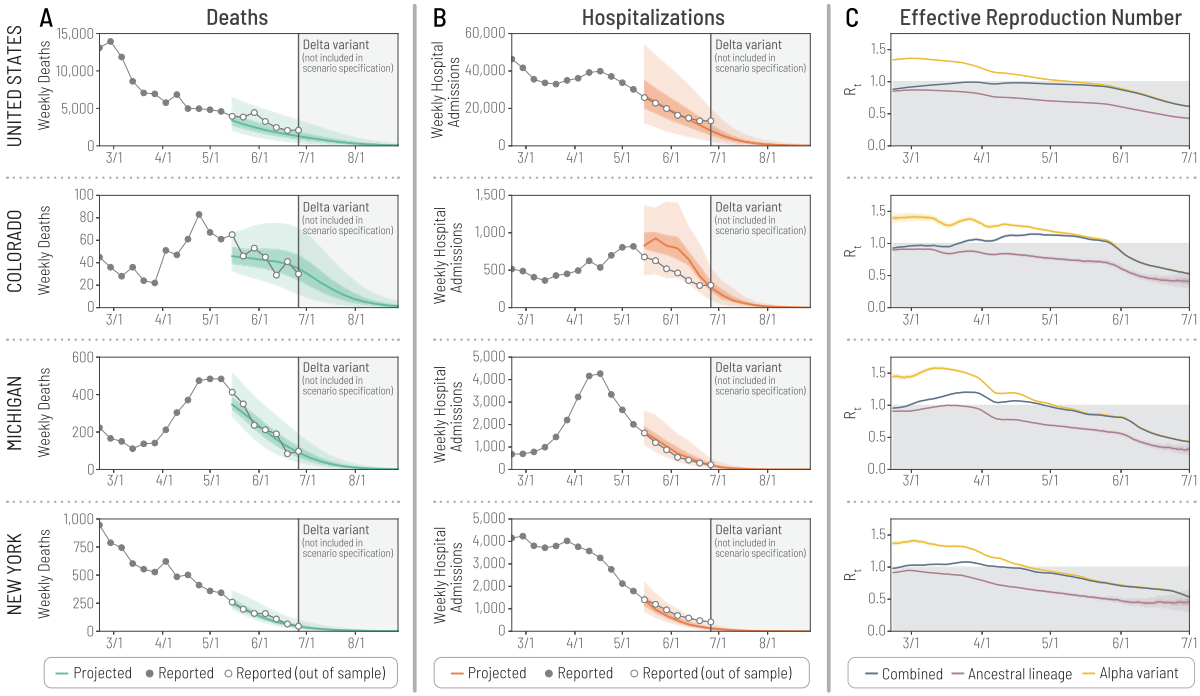

Fig. 3. (A) Out of sample model projections of weekly reported deaths for the US and selected states until June 28, 2022. The solid lines represent the median values, the darker shaded regions the IQR and the lighter shaded regions the 95% reference range. (B) Out of sample model projections of weekly hospital admissions for the US. The solid lines represent the median values, the darker shaded regions the IQR and the lighter shaded regions the 95% reference range. (C) R_t estimates for the US and selected states. The solid lines represent the median values and the lighter shaded regions the 95% reference range.

likely due to the relatively short assessment window of six weeks. Additional rounds of the SMH are evaluated for the most plausible scenarios in the SI. A comprehensive discussion of the performance evaluation of scenario projections is provided in Howerton et al. (2023) and in this issue (Bay et al., 2023).

In analyzing the performance of our models, it is however crucial to recognize that both the baseline and the four-weeks ahead forecast models are not naive in their design. These models undergo weekly revisions incorporating updates in surveillance data and changes in contact and mobility levels. This iterative updating process sets them apart from scenario projections. Unlike the forecast models, scenario projections are based on a set of initial assumptions and do not adjust on the basis of new information gathered in the out-of-sample regime.

3.2. The dynamics of the alpha variant

To analyze the evolution of the Alpha variant across the US, we focus on the scenario assumptions of the high vaccination scenario and ensemble the moderate and low NPIs together, assuming a future decline in NPIs effectiveness ranging from 50% to 80%. These two scenarios can be regarded *a posteriori* as the most plausible scenarios, meaning they closely align with the actual occurrence. In Fig. 3A and B we show the results of the out-of-sample projections for 7 weeks of the weekly number of deaths and hospitalizations for the US and selected states (see SI for all states). In the figure, the out-of-sample data are considered up to June 28, 2021, after that date the epidemic trajectory shows the emergence of the Delta variant (lineage B1.617.2), which was not considered in the scenario design. Our projections align with the trajectories of the deaths and hospitalizations that capture the decline of Alpha wave.

With a two-strain model we can distinguish between the infections that are generated from the ancestral lineage and Alpha variant separately. Using the daily time series of new infections per lineage, we can disentangle the contribution of each lineage to the effective reproduction number, R_t. The effective reproduction number represents the average number of secondary infections generated by a single infected individual at time t. The R_t value is a useful metric because it is affected by factors such as population immunity and behavioral changes (e.g., NPIs). In Fig. 3C we report the effective reproduction number R_t of each lineage, including the overall R_t for the US and selected states (see SI for all states). The R_t was estimated using a Bayesian approach on the time series of the daily new infectious individuals for each lineage taken from the median estimates of the calibrated model (Zhang et al., 2020). We observed large heterogeneity's across states in the behavior of the overall effective reproduction number.

As the more transmissible variant spreads, its prevalence, P, defined as the proportion of infections generated by that variant, increases which could result in an increase in the overall effective reproduction number. However, other factors such as population immunity, vaccination prevalence, and NPIs could limit the disease burden of the more transmissible lineage. Across the US we find a heterogeneous burden of the Alpha wave. It is also important to stress that a more transmissible variant is bound to become dominant even if the overall number of cases is decreasing and the overall effective reproductive number is smaller than one. This is evident for a number of states where the increase of the Alpha variant was not associated with a sustained increase in epidemic activity.

While a full mechanistic understanding of the dynamics of multiple strains is beyond the scope of this study, it is possible to use a simple two-strain deterministic model with full cross-protection to obtain the expression for the early growth of the prevalence of the more transmissible strain as

$$P(t) \simeq e^{\mu\psi R_{\hat{i}}(t-t_0)}, \tag{3}$$

where $R_{\hat{i}}$ is the effective reproductive number of the dominant and less transmissible strain during the initial introduction and spread of the new variant (during the time window $\hat{i}$) and is assumed to be constant, t_0 is the time of introduction, and μ is the generation time assumed to be the same for both strains (a full derivation of this result and its assumptions are reported in the SI). This expression shows

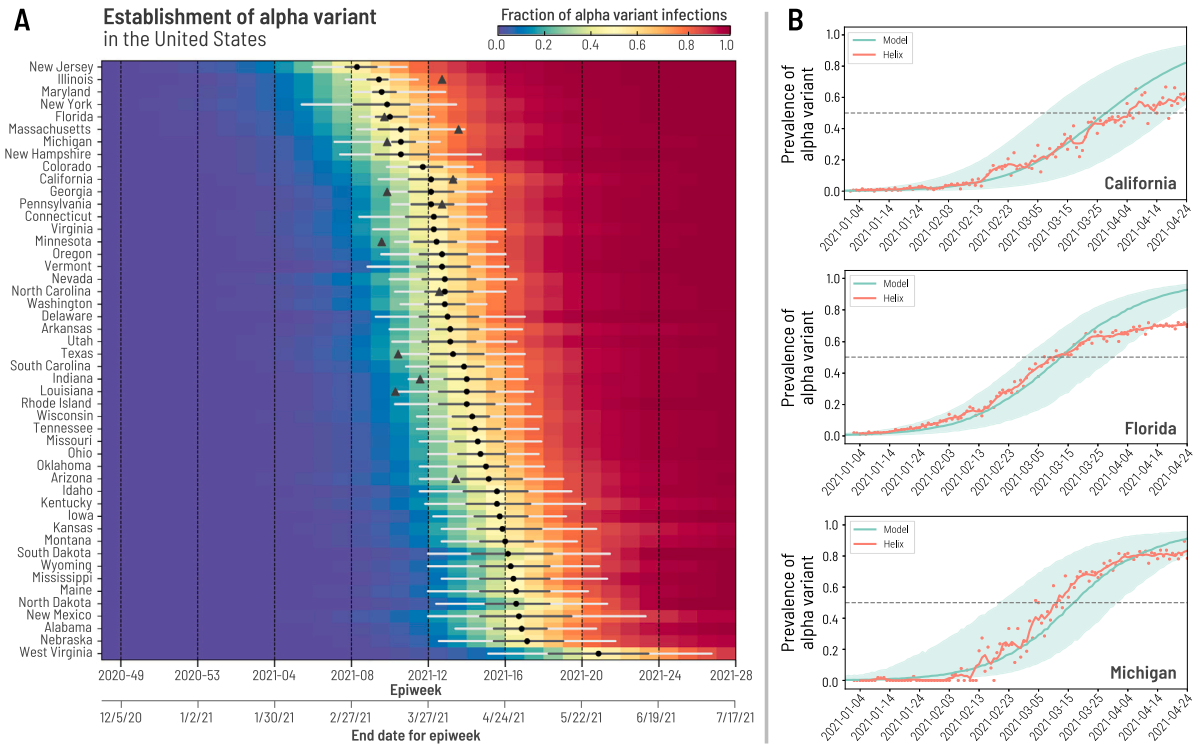

Fig. 4. (A) Weekly fraction of infections due to the Alpha variant for each state as a function of time for each state in the contiguous US. The black circles indicate the median day the variant becomes dominant. The gray lines indicate the IQR and the white lines the 90% reference range. The triangles show when the variant became dominant for some states according to the Helix data source (Helix, 2021). (B) Fraction of cases due to the Alpha variant over time for: California, Florida, and Michigan. The green line (median) and the shaded areas (90%RR) are the results projected by our model. The orange circles are the reported Helix data and the orange line corresponds to the 5-day moving average. (For interpretation of the references to color in this figure legend, the reader is referred to the web version of this article.)

that the emergence of a more transmissible strain's dominance can be highly variable across geographic regions, contingent upon the timing of its introduction and the local effective reproductive numbers of the ancestral strain, which in turn depend on factors such as NPIs, residual immunity, and vaccination rates that vary among different states.

3.3. The introduction and establishment of the alpha variant

In our study, we used a compartmental structure specifically designed as a two-strain model that intentionally excludes direct genomic data integration. This decision was made to prioritize the validation of the simulated epidemiological dynamics, enabling the model to effectively characterize the general behaviors of multiple viral strains without relying on detailed genomic information. During the calibration process, specific data on the growth and prevalence of the Alpha variant were not incorporated. Remarkably, despite the absence of direct genomic data, our model is capturing the prevalence trends of the Alpha variant over time. Indeed, the multiscale modeling approach used here leverages the international travel patterns that drive the initial dispersion and introduction of the Alpha variant. Our results show that the amount of international travel generated by the global transportation network is strongly associated to the initial seeding time of the Alpha lineage (see SI). However, the internal mobility and contact patterns at the county level, which are integrated into the mechanistic structure of the multiscale model, highlight that the local factors play a critical role in the spread of the Alpha variant as it competes with the ancestral lineage. This result parallels findings concerning the heterogeneities in the initial introduction of SARS-CoV-2 to the US during the beginning of the COVID-19 pandemic (Davis et al., 2021). The heterogeneities found here go beyond the simple expression reported in Eq. (3). Therefore, to study in detail the path to dominance of the Alpha variant across the US, we calculate time-varying prevalence of the Alpha lineage according to our model. We define the time of dominance as the date when the prevalence of the variant exceeds 50%; i.e. more than half of the new infections are due to the Alpha variant.Fig. 4A shows the weekly fraction of infections due to the Alpha variant over time. The results highlight the heterogeneous paths towards dominance. The median estimates of the dominance times span three months across the states. Our results are in agreement with previously published projections that found that the variant would become dominant by the end of March 2021 (Davies et al., 2021; Galloway et al., 2021; Washington et al., 2021).

To further validate our results, we use data from the *The Helix COVID-19 Surveillance Dashboard* (Helix, 2021) that is based on S-gene target failure. The data reported by this dashboard include the state of residence, the date of collection of the sample, the number of positive tests results, the number of positive tests results with S gene target failure, the number of sequenced test results with S gene target failure, and the number of positive test results that were sequenced and known to be of the Alpha variant (for biases and limitations see Helix (2021)). By using these metrics, we can build a timeline of the prevalence of the Alpha variant for each state reported in the dataset and compare it to our estimates. In Fig. 4B, we compare the daily fraction of infections due to the variant from our model (median and 90% reference range) with the data from Helix for three states: California, Florida, and Michigan. The surveillance data from Helix generally fall within the confidence interval of our model. However, for some states, we observe a plateauing after reaching dominance which deviates from our results. This is due to other strains like the Gamma (or P.1) and Delta (or B.1.617.2) variants of concern increasing in prevalence, which are not included in our modeling scheme. In the SI, we show a comparison for all states reported by Helix with a statistically significant number of samples.

We leverage the resolution of our model to study combined statistical areas (CSA, 2020). Our results at a higher geographical resolution confirm that the heterogeneity in reaching dominance is not only

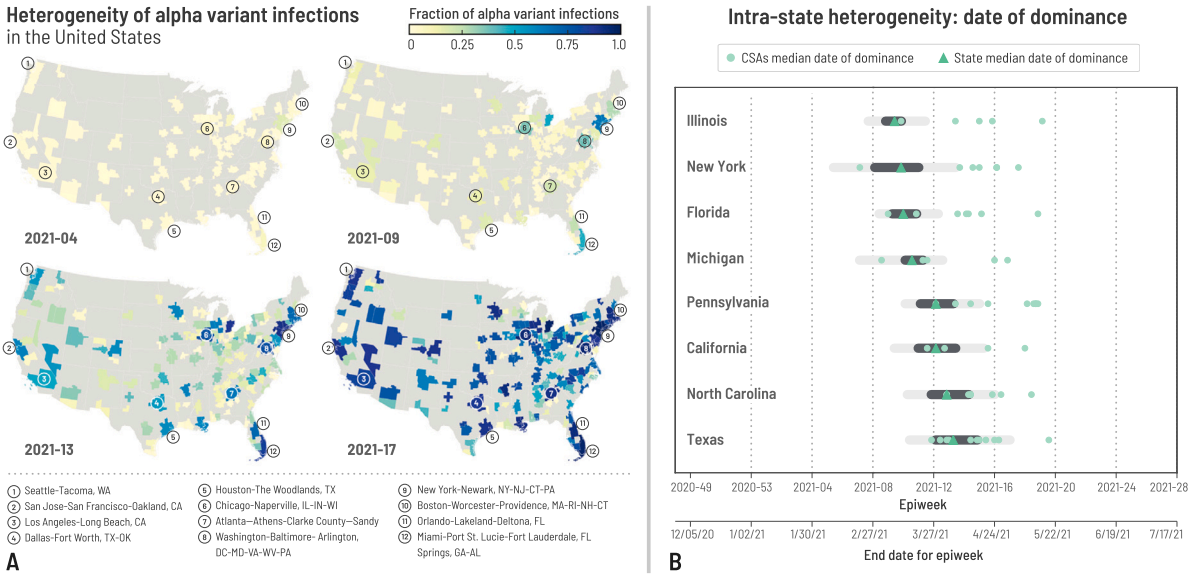

Fig. 5. (A) The fraction of Alpha variant infections during 4 different weeks across the US for all CSAs. (B) The time to dominance for selected states and their CSAs. The dark green triangles indicate the median date the variant becomes dominant in a given state and the dark (light) gray bars indicate the IQR (90% reference range). The light green circles indicate the median date the variant becomes dominant in a given CSA that is a part of that state. (For interpretation of the references to color in this figure legend, the reader is referred to the web version of this article.)

present at the state level but also when we look within a state. In Fig. 5A we show the dynamics of the prevalence of the Alpha variant across 4 selected weeks in early 2021. In early March (epiweek 2021–09), most CSAs have either no detections or a less than 25% prevalence of the Alpha variant according to the model except for a few high-traffic regions such as New York-Newark, NY-NJ-CT-PA, Chicago-Naperville, IL-IN-WI, and Miami-Port St. Lucie–Fort Lauderdale, FL Springs, GA-AL. Zooming in, in Fig. 5B, for states containing multiple CSAs, we find high intra-state heterogeneity with respect to the time of dominance of the Alpha variant. The results show that the heterogeneity is not only observed at the state level but also at CSA level. Interestingly, across all eight states, the week marking the dominance of the Alpha variant in several of their CSAs is outside (and mostly occurring after the median) the 90% reference range computed at the state level. However, some CSAs anticipate the state median. This is the case for Miami and New York. These two cities in particular are the location of two important international port-of-entries in the US that are associated with a large incoming flux of travelers as they have the first and third largest traffic volume in the US, respectively.

4. Discussion

As of March, 2023, the multiscale model presented here has been used to submit 17 rounds of projections to the SMH. Our approach has undergone many changes to adapt to the scenario specifications and variations in the epidemiological landscape. The model's calibration time window has also varied based on the SMH coordinating team's direction. Despite these changes, the basic geographical structure and resolution of the model have been maintained. Further details on how the epidemic transmission model and other parameters have changed can be found in the SI. Additionally, we report the performance of our model across 10 rounds by measuring the WIS for the projection period and calculating the ratio between the scores of two reference COVID-19 ensemble forecasting models. It is important to note that the initial conditions of the model were developed as scenarios and not with the goal of forecasting. The scenario projections are also analyzed over a longer time window, unlike the COVID-19 Forecasting Hub models which only forecast a maximum of 4 weeks ahead. For a full assessment of all rounds and models submitted to the SMH we refer the reader to Howerton et al. (2023).

The results concerning the introduction of the Alpha variant in the US indicate that the importation events were both temporally and spatially heterogeneous and determined by the source location's connectivity in the global transportation network. The initial importation events and the prevalence of the more transmissible Alpha variant progressed differently across various locations due to the changes in mobility patterns, the distribution of population, and the strength of NPIs. The initial importation of variants into different regions of the US are linked to the global airline traffic determining the entry points and early spread patterns of the virus. Furthermore, international transportation hubs generally resides in areas with high population densities with densely interconnected local mobility (commuting) networks. These networks in their turn contribute to the disease spread in nearby regions. Finally, the strength and adherence to NPIs also varied considerably, further contributing to the heterogeneous dynamic of variants. Specifically our model indicates that these factors led to considerable differences in the time when the Alpha variant became the dominant strain, ranging across states from March to May, 2021. Leveraging the resolution of the model we also studied results at the level of CSAs. In doing so, we uncover high heterogeneities even within states. CSAs featuring high mobility fluxes and populations experienced an early growth of infections caused by the new variant with respect to less populated and more secluded areas (when considering within state results). This is evident in the contrast between international travel hubs, where the Alpha variant dominance was noted as early as March, and more isolated regions, which saw a later dominance in mid-August.

Like all modeling approaches, our multiscale model has limitations and requires specific assumptions. Although two geographical levels of analysis are considered, there could be heterogeneity in the timing of variant establishment at even smaller scales. Moreover, when projecting scenarios, it is often challenging to obtain accurate information about the growth advantage of emerging variants, which can be attributed to increased transmissibility and/or immune escape (Volz, 2023). Assumptions about how to handle this growth advantage at the mechanistic level can generate different results on long-term projections. Additionally, changes in characteristic times such as the generation time, which are not always available at the moment of estimating the impact of an emerging variant, can also contribute to uncertainty. Furthermore, scenario modeling requires assumptions about vaccine

uptake, as well as changes in pathogen transmissibility due to population behavioral changes. Therefore, scenario projections should not be considered as a forecast of the epidemic's future trajectory but rather an attempt to bound possible future trajectories based on different assumptions.

Although the results presented here focused on a particular variant, the methodology can be extended to study how other, more transmissible strains can spread quickly, take over the share of new infections, and drastically alter the epidemic trajectory even during a successful vaccine rollout. While modeling approaches cannot replace ground truth data, mechanistic modeling frameworks can complement genomic surveillance efforts to track the unfolding of variants of concern and model their introduction, establishment, and path to dominance at a fine-grained geographical scale.

Code availability

The GLEAM model is publicly available at http://www.gleamviz.org/.

CRediT authorship contribution statement

Matteo Chinazzi: Data curation, Investigation, Writing – original draft. **Jessica T. Davis:** Data curation, Investigation, Writing – original draft. **Ana Pastore y Piontti:** Data curation, Investigation, Writing – original draft. **Kunpeng Mu:** Data curation, Investigation, Writing – original draft. **Nicolò Gozzi:** Investigation, Writing – original draft. **Marco Ajelli:** Investigation, Writing – original draft. **Nicola Perra:** Investigation, Writing – original draft. **Alessandro Vespignani:** Data curation, Investigation, Writing – original draft.

Declaration of competing interest

The authors declare that they have no known competing financial interests or personal relationships that could have appeared to influence the work reported in this paper.

Data availability

Epidemic surveillance data were collected from the Johns Hopkins Coronavirus Resource Center https://coronavirus.jhu.edu/. Proprietary airline data are commercially available from OAG (https://www.oag.com/) and IATA (https://www.iata.org/) databases. Other model intervention data includes Google's COVID-19 Community Mobility Reports available at https://www.google.com/covid19/mobility/ and the Oxford COVID-19 Response Tracker available at https://github.com/OxCGRT/covid-policy-tracker.

Acknowledgments

MC, MA, JTD, KM, APP and AV acknowledge support from COVID Supplement CDC-HHS-6U01IP001137-01, and the Cooperative Agreement no. NU38OT000297 from the Council of State and Territorial Epidemiologists (CSTE) and the CDC-75D301Cl4810 contract. MC acknowledges support from CDC-JHU-2005702123. MC and AV acknowledge support from Google Cloud and Google Cloud Research Credits program to fund this project. The findings and conclusions in this study are those of the authors and do not necessarily represent the official position of the funding agencies, the National Institutes of Health, United States, or the U.S. Department of Health and Human Services, United States.

Appendix A. Supplementary data

Supplementary material related to this article can be found online at https://doi.org/10.1016/j.epidem.2024.100757.

References

Balcan, D., Colizza, V., Gonçalves, B., Hu, H., Ramasco, J.J., Vespignani, A., 2009. Multiscale mobility networks and the spatial spreading of infectious diseases. Proc. Natl. Acad. Sci. 106 (51), 21484–21489. http://dx.doi.org/10.1073/pnas.0906910106.

Balcan, D., Gonçalves, B., Hu, H., Ramasco, J.J., Colizza, V., Vespignani, A., 2010. Modeling the spatial spread of infectious diseases: The global epidemic and mobility computational model. J. Comput. Sci. 1 (3), 132–145. http://dx.doi.org/10.1016/j.jocs.2010.07.002.

Balcan, D., Vespignani, A., 2011. Phase transitions in contagion processes mediated by recurrent mobility patterns. Nat. Phys. 7, 581–586. http://dx.doi.org/10.1038/nphys1944.

Bay, C., St-Onge, G., Davis, J.T., Chinazzi, M., Howerton, E., Lessler, J., Runge, M.C., Shea, K., Truelove, S., Viboud, C., Vespignani, A., 2023. Ensemble2: Scenarios ensembling for communication and performance analysis. Epidemics 46, 100748. http://dx.doi.org/10.1016/j.epidem.2024.100748.

Beaumont, M.A., Zhang, W., Balding, D.J., 2002. Approximate Bayesian computation in population genetics. Genetics 162 (4), 2025–2035, https://www.genetics.org/content/162/4/2025.

Biggerstaff, M., Slayton, R.B., Johansson, M.A., Butler, J.C., 2022. Improving pandemic response: Employing mathematical modeling to confront Coronavirus disease 2019. Clin. Infect. Dis. 74 (5), 913–917. http://dx.doi.org/10.1093/cid/ciab673.

Borchering, R.K., Mullany, L.C., Howerton, E., Chinazzi, M., Smith, C.P., Qin, M., Reich, N.G., Contamin, L., Levander, J., Kerr, J., Espino, J., Hochheiser, H., Lovett, K., Kinsey, M., Tallaksen, K., Wilson, S., Shin, L., Lemaitre, J.C., Hulse, J.D., Kaminsky, J., Lee, E.C., Hill, A.L., Davis, J.T., Mu, K., Xiong, X., Piontti, A.P.y., Vespignani, A., Srivastava, A., Porebski, P., Venkatramanan, S., Adiga, A., Lewis, B., Klahn, B., Outten, J., Hurt, B., Chen, J., Mortveit, H., Wilson, A., Marathe, M., Hoops, S., Bhattacharya, P., Machi, D., Chen, S., Paul, R., Janies, D., Thill, J.-C., Galanti, M., Yamana, T., Pei, S., Shaman, J., España, G., Cavany, S., Moore, S., Perkins, A., Healy, J.M., Slayton, R.B., Johansson, M.A., Biggerstaff, M., Shea, K., Truelove, S.A., Runge, M.C., Viboud, C., Lessler, J., 2023. Impact of SARS-CoV-2 vaccination of children ages 5–11 years on COVID-19 disease burden and resilience to new variants in the united states, november 2021–march 2022: A multi-model study. Lancet Regional Health – Am. 17, 100398. http://dx.doi.org/10.1016/j.lana.2022.100398.

Borchering, R.K., Viboud, C., Howerton, E., et al., 2021. Modeling of future COVID-19 cases, hospitalizations, and deaths, by vaccination rates and nonpharmaceutical intervention scenarios — United states, april–september 2021. MMWR. Morbidity Mortality Weekly Rep. 70, 719–724. http://dx.doi.org/10.15585/mmwr.mm7019e3.

Bracher, J., Ray, E.L., Gneiting, T., Reich, N.G., 2021. Evaluating epidemic forecasts in an interval format. PLoS Comput. Biol. 17 (2), e1008618. http://dx.doi.org/10.1371/journal.pcbi.1008618.

Brooks-Pollock, E., Danon, L., Jombart, T., Pellis, L., 2021. Modelling that shaped the early COVID-19 pandemic response in the UK. Philos. Trans. R. Soc. B 376 (1829), 20210001. http://dx.doi.org/10.1098/rstb.2021.0001.

CDC, 2021 COVID-19 Vaccinations in the United States. https://covid.cdc.gov/covid-data-tracker/vaccinations_vacc-total-admin-rate-total".

Chinazzi, M., Davis, J.T., Ajelli, M., Gioannini, C., Litvinova, M., Merler, S., y Piontti, A.P., Mu, K., Rossi, L., Sun, K., et al., 2020. The effect of travel restrictions on the spread of the 2019 novel Coronavirus (COVID-19) outbreak. Science 368 (6489), 395–400. http://dx.doi.org/10.1126/science.aba9757.

COVID-19 Scenario Modeling Hub, 2021. Round 5 scenario specifications. https://github.com/midas-network/covid19-scenario-modeling-hub/blob/master/previous-rounds/README_Round5.md.

Cramer, E.Y., Huang, Y., Wang, Y., Ray, E.L., Cornell, M., Bracher, J., Brennen, A., Rivadeneira, A.J.C., Gerding, A., House, K., Jayawardena, D., Kanji, A.H., Khandelwal, A., Le, K., Mody, V., Mody, V., Niemi, J., Stark, A., Shah, A., Wattanchit, N., Zorn, M.W., Reich, N.G., 2022. The united states COVID-19 forecast hub dataset. Sci. Data 9 (1), 462. http://dx.doi.org/10.1038/s41597-022-01517-w.

CSA, 2020. Combined Statistical Areas. https://www.census.gov/geographies/reference-maps/2020/geo/csa.html. (Accessed 27 May 2021).

Davies, N.G., Abbott, S., Barnard, R.C., Jarvis, C.I., Kucharski, A.J., Munday, J.D., Pearson, C.A., Russell, T.W., Tully, D.C., Washburne, A.D., et al., 2021. Estimated transmissibility and impact of SARS-CoV-2 lineage B. 1.1. 7 in England. Science 372 (6538), http://dx.doi.org/10.1126/science.abg3055, eabg3055.

Davis, J.T., Chinazzi, M., Perra, N., Mu, K., Pastore y Piontti, A., Ajelli, M., Dean, N.E., Gioannini, C., Litvinova, M., Merler, S., Rossi, L., Sun, K., Xiong, X., Longini, I.M., Halloran, M., Viboud, C., Vespignani, A., 2021. Cryptic transmission of SARS-CoV-2 and the first COVID-19 wave. Nature 600 (7887), 127–132. http://dx.doi.org/10.1038/s41586-021-04130-w.

Dong, E., Du, H., Gardner, L., 2020. An interactive web-based dashboard to track COVID-19 in real time. Lancet Infect. Dis. 20 (5), 533–534. http://dx.doi.org/10.1016/S1473-3099(20)30120-1.

Dooling, K., McClung, N., Chamberland, M., et al., 2020. The advisory committee on immunization practices' interim recommendation for allocating initial supplies of COVID-19 vaccine — United states, 2020. MMWR. Morbidity Mortality Weekly Rep. 69, 1857–1859. http://dx.doi.org/10.15585/mmwr.mm6949e1, URL https://www.cdc.gov/mmwr/volumes/69/wr/mm6949e1.htm.

Galloway, S.E., Paul, P., MacCannell, D.R., Johansson, M.A., Brooks, J.T., MacNeil, A., Slayton, R.B., Tong, S., Silk, B.J., Armstrong, G.L., et al., 2021. Emergence of SARS-CoV-2 b.1.1.7 lineage—United States, december 29, 2020–january 12, 2021. Morbidity Mortality Weekly Rep. 70 (3), 95. http://dx.doi.org/10.15585/mmwr.mm7003e2.

Gneiting, T., Raftery, A.E., 2007. Strictly proper scoring rules, prediction, and estimation. J. Amer. Statist. Assoc. 102 (477), 359–378. http://dx.doi.org/10.1198/016214506000001437, Publisher: Taylor & Francis _eprint: 10.1198/016214506000001437.

Gomes, M.F.C., Pastore y Piontti, A., Rossi, L., Chao, D., Longini, I., Halloran, M.E., Vespignani, A., 2014. Assessing the international spreading risk associated with the 2014 west African Ebola outbreak. PLoS Currents 6, http://dx.doi.org/10.1371/currents.outbreaks.cd818f63d40e24aef769dda7df9e0da5, URL https://www.ncbi.nlm.nih.gov/pmc/articles/PMC4169359/.

Google LLC, 2021a. Google COVID-19 community mobility reports. https://www.google.com/covid19/mobility/.

Google LLC, 2021b. Google COVID-19 community mobility reports: Mobility report CSV documentation. https://www.google.com/covid19/mobility/data_documentation.html?hl=en.

Hale, T., Angrist, N., Goldszmidt, R., Kira, B., Petherick, A., Phillips, T., Webster, S., Cameron-Blake, E., Hallas, L., Majumdar, S., Tatlow, H., 2021. A global panel database of pandemic policies (Oxford COVID-19 government response tracker). Nat. Hum. Behav. 5 (4), 529–538. http://dx.doi.org/10.1038/s41562-021-01079-8.

Helix, 2021. Data sourced from the Helix® COVID-19 surveillance dashboard. https://www.helix.com/pages/helix-covid-19-surveillance-dashboard. (Accessed 18 May 2021).

Holmdahl, I., Buckee, C., 2020. Wrong but useful — What Covid-19 epidemiologic models can and cannot tell us. N. Engl. J. Med. 383 (4), 303–305. http://dx.doi.org/10.1056/NEJMp2016822.

Howerton, E., Contamin, L., Mullany, L.C., Qin, M., Reich, N.G., Bents, S., Borchering, R.K., Jung, S.-m., Loo, S.L., Smith, C.P., Levander, J., Kerr, J., Espino, J., Panhuis, W.G.v., Hochheiser, H., Galanti, M., Yamana, T., Pei, S., Shaman, J., Rainwater-Lovett, K., Kinsey, M., Tallaksen, K., Wilson, S., Shin, L., Lemaitre, J.C., Kaminsky, J., Hulse, J.D., Lee, E.C., McKee, C., Hill, A., Karlen, D., Chinazzi, M., Davis, J.T., Mu, K., Xiong, X., Piontti, A.P.y., Vespignani, A., Rosenstrom, E.T., Ivy, J.S., Mayorga, M.E., Swann, J.L., España, G., Cavany, S., Moore, S., Perkins, A., Hladish, T., Pillai, A., Toh, K.B., Longini, I., Chen, S., Paul, R., Janies, D., Thill, J.-C., Bouchnita, A., Bi, K., Lachmann, M., Fox, S., Meyers, L.A., Consortium, U.C.-.M., Srivastava, A., Porebski, P., Venkatramanan, S., Adiga, A., Lewis, B., Klahn, B., Outten, J., Hurt, B., Chen, J., Mortveit, H., Wilson, A., Marathe, M., Hoops, S., Bhattacharya, P., Machi, D., Cadwell, B.L., Healy, J.M., Slayton, R.B., Johansson, M.A., Biggerstaff, M., Truelove, S., Runge, M.C., Shea, K., Viboud, C., Lessler, J., 2023. Evaluation of the us covid-19 scenario modeling hub for informing pandemic response under uncertainty. Nature communications 14 (1), 7260. http://dx.doi.org/10.1038/s41467-023-42680-x.

Jewell, N.P., Lewnard, J.A., Jewell, B.L., 2020. Predictive mathematical models of the COVID-19 pandemic: Underlying principles and value of projections. JAMA 323 (19), 1893–1894. http://dx.doi.org/10.1001/jama.2020.6585.

Mistry, D., Litvinova, M., Chinazzi, M., Fumanelli, L., Gomes, M.F., Haque, S.A., Liu, Q.-H., Mu, K., Xiong, X., Halloran, M.E., et al., 2021. Inferring high-resolution human mixing patterns for disease modeling. Nature Commun. 12 (1), 323. http://dx.doi.org/10.1038/s41467-020-20544-y.

NERVTAG, 2020. NERVTAG meeting on SARS-CoV-2 variant under investigation VUI-202012/01. (Online; Accessed 21 December 2020).

OAG, 2020. Official aviation guide. https://www.oag.com/.

Our World in Data, 2021, State-by-state data on COVID-19 vaccinations in the United States. https://ourworldindata.org/us-states-vaccinations.

PHE, 2021. Investigation of novel SARS-CoV-2 variant. Variant of concern 202012/01. Technical briefing 3. https://assets.publishing.service.gov.uk/government/uploads/system/uploads/attachment_data/file/950823/Variant_of_Concern_VOC_202012_01_Technical_Briefing_3_-_England.pdf. (Online; Accessed 13 January 2021).

Pilishvili, T., Fleming-Dutra, K.E., Farrar, J.L., Gierke, R., Mohr, N.M., Talan, D.A., Krishnadasan, A., Harland, K.K., Smithline, H.A., Hou, P.C., Lee, L.C., Lim, S.C., Moran, G.J., Krebs, E., Steele, M., Beiser, D.G., Faine, B., Haran, J.P., Nandi, U., Schrading, W.A., Chinnock, B., Henning, D.J., LoVecchio, F., Nadle, J., Barter, D., Brackney, M., Britton, A., Marceaux-Galli, K., Lim, S., Phipps, E.C., Dumyati, G., Pierce, R., Markus, T.M., Anderson, D.J., Debes, A.K., Lin, M., Mayer, J., Babcock, H.M., Safdar, N., Fischer, M., Singleton, R., Chea, N., Magill, S.S., Verani, J., Schrag, S., Team, V.E.A.H.P.S., 2021. Interim estimates of vaccine effectiveness of Pfizer-BioNTech and moderna COVID-19 vaccines among health care personnel — 33 U.S. sites, january–march 2021. MMWR Weekly 70, 753–758. http://dx.doi.org/10.15585/mmwr.mm7020e2externalicon, On May 14, 2021, this report was posted online as an MMWR Early Release. This report has been corrected.

Pastore y Piontti, A., Perra, N., Rossi, L., Samay, N., Vespignani, A., 2018. Charting the Next Pandemic: Modeling Infectious Disease Spreading in the Data Science Age. Springer, http://dx.doi.org/10.1007/978-3-319-93290-3.

Pastore y Piontti, A., Zhang, Q., Gomes, M.F.C., Rossi, L., Poletto, C., Colizza, V., Chao, D.L., Longini, I.M., Halloran, M.E., Vespignani, A., 2016. Real-time assessment of the international spreading risk associated with the 2014 west African Ebola outbreak. In: Chowell, G., Hyman, J.M. (Eds.), Mathematical and Statistical Modeling for Emerging and Re-Emerging Infectious Diseases. Springer International Publishing, Cham, pp. 39–56. http://dx.doi.org/10.1007/978-3-319-40413-4_4.

Polack, F.P., Thomas, S.J., Kitchin, N., Absalon, J., Gurtman, A., Lockhart, S., Perez, J.L., Pérez Marc, G., Moreira, E.D., Zerbini, C., Bailey, R., Swanson, K.A., Roychoudhury, S., Koury, K., Li, P., Kalina, W.V., Cooper, D., Frenck, R.W., Hammitt, L.L., Türeci, Ö., Nell, H., Schaefer, A., Ünal, S., Tresnan, D.B., Mather, S., Dormitzer, P.R., Şahin, U., Jansen, K.U., Gruber, W.C., 2020. Safety and efficacy of the BNT162b2 mRNA Covid-19 vaccine. N. Engl. J. Med. 383 (27), 2603–2615. http://dx.doi.org/10.1056/NEJMoa2034577.

Poletto, C., Scarpino, S.V., Volz, E.M., 2020. Applications of predictive modelling early in the COVID-19 epidemic. Lancet. Digit. Health 2 (10), e498–e499. http://dx.doi.org/10.1016/S2589-7500(20)30196-5, URL https://www.ncbi.nlm.nih.gov/pmc/articles/PMC7417175/.

Prem, K., Cook, A.R., Jit, M., 2017. Projecting social contact matrices in 152 countries using contact surveys and demographic data. PLoS Comput. Biol. 13 (9), e1005697. http://dx.doi.org/10.1371/journal.pcbi.1005697.

Rambaut, A., Loman, N., Pybus, O., Barclay, W., Barrett, J., Carabelli, A., Connor, T., Peacock, T., Robertson, D.L., Volz, E., COVID-19 Genomics Consortium UK (CoG-UK), 2020. Preliminary genomic characterisation of an emergent SARS-CoV-2 lineage in the UK defined by a novel set of spike mutations. https://virological.org/t/preliminary-genomic-characterisation-of-an-emergent-sars-cov-2-lineage-in-the-uk-defined-by-a-novel-set-of-spike-mutations/563.

Reich, N.G., Lessler, J., Funk, S., Viboud, C., Vespignani, A., Tibshirani, R.J., Shea, K., Schienle, M., Runge, M.C., Rosenfeld, R., Ray, E.L., Niehus, R., Johnson, H.C., Johansson, M.A., Hochheiser, H., Gardner, L., Bracher, J., Borchering, R.K., Biggerstaff, M., 2022. Collaborative hubs: Making the most of predictive epidemic modeling. Am J Public Health 112 (6), 839–842. http://dx.doi.org/10.2105/AJPH.2022.306831.

Salje, H., Kiem, C.T., Lefrancq, N., Courtejoie, N., Bosetti, P., Paireau, J., Andronico, A., Hozé, N., Richet, J., Dubost, C.-L., Strat, Y.L., Lessler, J., Levy-Bruhl, D., Fontanet, A., Opatowski, L., Boelle, P.-Y., Cauchemez, S., 2020. Estimating the burden of SARS-CoV-2 in France. Science 369 (6500), 208–211. http://dx.doi.org/10.1126/science.abc3517.

Scenario Modeling Hub, 2023. COVID-19 scenario modeling hub. https://covid19scenariomodelinghub.org/.

Science Magazine, 2020. Mutant Coronavirus in the United Kingdom sets off alarms, but its importance remains unclear. https://www.sciencemag.org/news/2020/12/mutant-coronavirus-united-kingdom-sets-alarms-its-importance-remains-unclear. (Online; Accessed 21 December 2020).

Shapiro, J., Dean, N.E., Madewell, Z.J., Yang, Y., Halloran, M.E., Longini, I., 2021. Efficacy estimates for various COVID-19 vaccines: What we know from the literature and reports. http://dx.doi.org/10.1101/2021.05.20.21257461, medRxiv. URL https://www.medrxiv.org/content/10.1101/2021.05.20.21257461v2.

Sunnåker, M., Busetto, A.G., Numminen, E., Corander, J., Foll, M., Dessimoz, C., 2013. Approximate Bayesian computation. PLoS Comput. Biol. 9 (1), 1–10. http://dx.doi.org/10.1371/journal.pcbi.1002803.

Truelove, S., Smith, C.P., Qin, M., Mullany, L.C., Borchering, R.K., Lessler, J., Shea, K., Howerton, E., Contamin, L., Levander, J., Kerr, J., Hochheiser, H., Kinsey, M., Tallaksen, K., Wilson, S., Shin, L., Rainwater-Lovett, K., Lemairtre, J.C., Dent, J., Kaminsky, J., Lee, E.C., Perez-Saez, J., Hill, A., Karlen, D., Chinazzi, M., Davis, J.T., Mu, K., Xiong, X., Pastore y Piontti, A., Vespignani, A., Srivastava, A., Porebski, P., Venkatramanan, S., Adiga, A., Lewis, B., Klahn, B., Outten, J., Orr, M., Harrison, G., Hurt, B., Chen, J., Vullikanti, A., Marathe, M., Hoops, S., Bhattacharya, P., Machi, D., Chen, S., Paul, R., Janies, D., Thill, J.-C., Galanti, M., Yamana, T.K., Pei, S., Shaman, J.L., Healy, J.M., Slayton, R.B., Biggerstaff, M., Johansson, M.A., Runge, M.C., Viboud, C., 2022. Projected resurgence of COVID-19 in the United States in july—December 2021 resulting from the increased transmissibility of the delta variant and faltering vaccination. eLife 11, e73584. http://dx.doi.org/10.7554/eLife.73584.

US Census Bureau, 2024, 2011–2015 5-Year ACS Commuting Flows. https://www.census.gov/data/tables/2015/demo/metro-micro/commuting-flows-2015.html.

US Department of Health & Human Services, 2021, COVID-19 Reported Patient Impact and Hospital Capacity by State Timeseries. https://healthdata.gov/Hospital/COVID-19-Reported-Patient-Impact-and-Hospital-Capa/g62h-syeh.

Verity, R., Okell, L.C., Dorigatti, I., Winskill, P., Whittaker, C., Imai, N., Cuomo-Dannenburg, G., Thompson, H., Walker, P.G.T., Fu, H., Dighe, A., Griffin, J.T., Baguelin, M., Bhatia, S., Boonyasiri, A., Cori, A., Cucunubá, Z., FitzJohn, R., Gaythorpe, K., Green, W., Hamlet, A., Hinsley, W., Laydon, D., Nedjati-Gilani, G., Riley, S., van Elsland, S., Volz, E., Wang, H., Wang, Y., Xi, X., Donnelly, C.A., Ghani, A.C., Ferguson, N.M., 2020. Estimates of the severity of Coronavirus disease 2019: A model-based analysis. Lancet Infect. Dis. 20 (6), 669–677. http://dx.doi.org/10.1016/S1473-3099(20)30243-7.

Volz, E., 2023. Fitness, growth and transmissibility of SARS-CoV-2 genetic variants. Nature Rev. Genet. 24 (10), 724–734. http://dx.doi.org/10.1038/s41576-023-00610-z.

Walensky, R.P., Walke, H.T., Fauci, A.S., 2021. SARS-CoV-2 variants of concern in the United States—Challenges and opportunities. JAMA 325 (11), 1037–1038.

Washington, N.L., Gangavarapu, K., Zeller, M., Bolze, A., Cirulli, E.T., Barrett, K.M.S., Larsen, B.B., Anderson, C., White, S., Cassens, T., Jacobs, S., Levan, G., Nguyen, J., Ramirez, J.M., Rivera-Garcia, C., Sandoval, E., Wang, X., Wong, D., Spencer, E.,

Robles-Sikisaka, R., Kurzban, E., Hughes, L.D., Deng, X., Wang, C., Servellita, V., Valentine, H., Hoff, P.D., Seaver, P., Sathe, S., Gietzen, K., Sickler, B., Antico, J., Hoon, K., Liu, J., Harding, A., Bakhtar, O., Basler, T., Austin, B., MacCannell, D., Isaksson, M., Febbo, P.G., Becker, D., Laurent, M., McDonald, E., Yeo, G.W., Knight, R., Laurent, L.C., Feo, E.d., Worobey, M., Chiu, C.Y., Suchard, M.A., Lu, J.T., Lee, W., Andersen, K.G., 2021. Emergence and rapid transmission of SARS-CoV-2 B.1.1.7 in the united states. Cell 184 (10), 2587–2594.e7. http://dx.doi.org/10.1016/j.cell.2021.03.052, Publisher: Elsevier. URL https://www.cell.com/cell/abstract/S0092-8674(21)00383-4.

WHO, 2020. SARS-CoV-2 variant – United Kingdom of great Britain and Northern Ireland. https://www.who.int/csr/don/21-december-2020-sars-cov2-variant-united-kingdom/en/. (Online; Accessed 21 December 2020).

World Health Organization, 2021. Tracking SARS-CoV-2 variants. https://www.who.int/en/activities/tracking-SARS-CoV-2-variants/. (Online; Accessed 24 June 2021).

Zhang, J., Litvinova, M., Wang, W., Wang, Y., Deng, X., Chen, X., Li, M., Zheng, W., Yi, L., Chen, X., Wu, Q., Liang, Y., Wang, X., Yang, J., Sun, K., Longini, I.M., Halloran, M.E., Wu, P., Cowling, B.J., Merler, S., Viboud, C., Vespignani, A., Ajelli, M., Yu, H., 2020. Evolving epidemiology and transmission dynamics of Coronavirus disease 2019 outside Hubei province, China: A descriptive and modelling study. Lancet Infect. Dis. 20 (7), 793–802. http://dx.doi.org/10.1016/S1473-3099(20)30230-9.

Zhang, Q., Sun, K., Chinazzi, M., Pastore Y Piontti, A., Dean, N.E., Rojas, D.P., Merler, S., Mistry, D., Poletti, P., Rossi, L., Bray, M., Halloran, M.E., Longini, I.M., Vespignani, A., 2017. Spread of Zika virus in the Americas. Proc. Natl. Acad. Sci. 114 (22), http://dx.doi.org/10.1073/pnas.1620161114.